Magnetism-dependent phonon anomaly in LaFeAsO observed via inelastic x-ray scattering

S. E. Hahn, G. S. Tucker, J.-Q. Yan, A. H. Said, B. M. Leu, R. W. McCallum, E. E. Alp, T. A. Lograsso, R. J. McQueeney, and B. N. Harmon

Magnetism dependent phonon anomaly in LaFeAsO observed via inelastic x-ray scattering

S. E. Hahn,[1, 2] G. S. Tucker,[1, 2] J.-Q. Yan,[3, 4] A. H. Said,[5] B. M. Leu,[5] R. W. McCallum,[2] E. E. Alp,[5] T. A. Lograsso,[2, 6] R. J. McQueeney,[1, 2] and B. N. Harmon[1, 2]

[1]*Department of Physics and Astronomy, Iowa State University, Ames, IA, 50011, USA*
[2]*Division of Materials Science and Engineering, Ames Laboratory US-DOE, Iowa State University, Ames, IA 50011, USA*
[3]*Materials Science and Technology Division, Oak Ridge National Laboratory, Oak Ridge, TN, 37831, USA*
[4]*Department of Materials and Engineering, The University of Tennessee, Knoxville, TN, 37996, USA*
[5]*Advanced Photon Source, Argonne National Laboratory, Argonne, IL 60439, USA*
[6]*Department of Materials Science and Engineering, Iowa State University, Ames, IA, 50011 USA*
(Dated: February 4, 2013)

The phonon dispersion was measured at room temperature along (0,0,L) in the tetragonal phase of LaFeAsO using inelastic x-ray scattering. Spin-polarized first-principles calculations imposing various types of antiferromagnetic order are in better agreement with the experimental results than nonmagnetic calculations, although the measurements were made well above the magnetic ordering temperature, T_N. Splitting observed between two A_{1g} phonon modes at 22 and 26 meV is only observed in spin-polarized calculations. Magneto-structural effects similar to those observed in the AFe_2As_2 materials are confirmed present in LaFeAsO. The presence of Fe-spin is necessary to find reasonable agreement of the calculations with the measured spectrum well above T_N. On-site Fe and As force constants show significant softening compared to nonmagnetic calculations, however an investigation of the real-space force constants associates the magnetoelastic coupling with a complex renormalization instead of softening of a specific pairwise force.

Despite rather convincing arguments that superconductivity in the AFe_2As_2 (A=Ca,Sr,Ba,Eu) and RFeAsO (R=La,Ce,Pr,Nd,Sm,Gd)-based compounds does not originate from conventional electron-phonon coupling,[1] these systems do display significant sensitivity to the lattice geometry. For example, the size of the Fe moment is sensitive to the lattice parameters and As position, as shown by Density Functional Theory (DFT) calculations. One thus expects strong magneto-structural coupling in these compounds.[2] Also, measurements of the room temperature phonon density-of-states (DOS) in LaFeAsO indicates some disagreement with non-spin-polarized DFT calculations.[3,4] Distinct features in the phonon DOS, likely associated with atomic displacements in the Fe-As plane, were observed at significantly lower energies than non-magnetic calculations suggest. It was noted (empirically) that softening of the Fe-As force constants by 30% brings the calculated phonon DOS into better agreement with the data.[5] Theoretical studies have shown that strong coupling between Fe magnetism and the As position leads to the softening of the Fe-As force constants, thereby explaining the observed phonon spectra.[6]

While these magnetostructural effects are well documented in the AFe_2As_2-based systems, it is not clear if the same effects are present in the RFeAsO system. One key example of this coupling in $CaFe_2As_2$ comes from the observation of a transition from the antiferromagnetic state to a non-magnetic "collapsed tetragonal" state under applied pressure.[7] In this case, a reduction of the c-axis lattice parameter by 9.5% is associated with the complete collapse of the Fe magnetic moment.[8]

The lattice vibrational frequencies associated with c-axis vibrations of Ca and As atoms in $CaFe_2As_2$ and $BaFe_2As_2$[9–11] have been shown by inelastic neutron and x-ray scattering to disagree with predictions of non-spin polarized DFT calculations. In particular, the energy splitting between c-axis phonon branches containing As displacements was found to be in strong disagreement with non-spin polarized calculations. Ultimately, spin-polarized calculations in the local spin density approximation that include the AFM order present at lower temperatures were required to bring the calculated phonon dispersion into better agreement with room temperature measurements.[2] Our group was able to confirm the role of magnetism in c-axis polarized Ca and As modes in $CaFe_2As_2$ using single-crystal inelastic x-ray scattering (IXS) measurements at the Advanced Photon Source (APS) in combination with spin-polarized calculations using the Perdew-Burke-Ernzerhof (PBE) exchange-correlation functional.[9]

The difficulty of synthesizing RFeAsO in single-crystalline form has prevented a quantitative confirmation of similar magneto-structural coupling across the AFe_2As_2 and RFeAsO systems. It might be expected that the presence of RO layers, which results in a larger spacing of the FeAs layers along the c-axis, might mitigate these effects to some degree. Measured Raman and infrared spectra of LaFeAsO and SmFeAsO, however, show the A_{1g} phonon mode containing As motion has a frequency that is 11-13% lower than predicted by DFT calculations.[12,13] Recently single crystal samples of RFeAsO have become available.[14] IXS phonon data was recently reported on $PrFeAsO_{0.9}$[5] and SmFeAsO[15] single-crystals and large discrepancies were observed between DFT calculations and the experimental data. Understanding why the A_{1g} mode is lower than that predicted by DFT calculations still requires a more detailed investigation. Determining the role of spin-phonon coupling requires a comparison of the IXS data to both spin-polarized and non-magnetic calculations. In our previous studies of $CaFe_2As_2$, investigation of the c-axis polarized logitudinal modes along (00L) provided the clearest evidence of strong spin-phonon coupling. In the RFeAsO system, measurements along (00L) also eliminate contributions from the overlapping B_{1g} mode, thereby allowing clearer discriminations of the anomalous effects of the A_1g. Thus far, the dispersion along (00L) has not been reported in previous work on the RFeAsO system.

LaFeAsO single crystals were synthesized in NaAs flux at ambient pressure as described elsewhere.[14] Inelastic x-ray scattering measurements were performed on the HERIX instrument at sector 30-ID-C of the Advanced Photon Source at Argonne National Laboratory with incident beam energy of 23.724 keV and with an energy resolution of 1.44 meV.[16,17] Scattering is described in terms of the tetragonal P4/nmm unit cell where $\mathbf{Q} = \frac{2\pi}{a}(h\mathbf{i} + k\mathbf{j}) + \frac{2\pi}{c}l\mathbf{k}$. The vectors $\mathbf{i}$, $\mathbf{j}$, and $\mathbf{k}$ are the fundamental translation unit vectors in real space. Below T_S=156K, the sample transforms to an orthorhombic structure with space group Cmma.[18,19] The relationship between the Miller indices in the tetragonal P4/nmm and orthorhombic Cmma phase are, $h = (H_o + K_o)$, $k = (H_o - K_o)$, and $l = L_o$.

Below the magnetic ordering temperature T_N=138K, the sample develops long-range spin-density wave (SDW) AFM order. The crystalline mosaic full-width-at-half-maximum (FWHM) is 0.2 degrees, which is less than the angular acceptance of the analyzer (0.6 degrees). The sample was mounted in the (hhl) plane in a displex for low temperature studies, and the displex was attached to a 4-circle diffractometer.

Based on previous studies of c-axis polarized phonons in $CaFe_2As_2$, we focused our study on phonon branches along the $(0,0,8+\xi)$ direction in the Brillouin zone. In order to study the dispersion and potential line broadening of the phonon modes, the scans were fit to several peaks using a pseudo-Voigt line profile. The normalized pseudo-Voigt function is given in Eqn. 1, where $f_G(x;\Gamma)$ and $f_L(x;\Gamma)$ are normalized Gaussian and Lorentzian functions respectively. The mixing parameter $\eta = 0.74$, and resolution FWHM $\Gamma = 1.44$ meV was determined from fits to the elastic scattering width of Plexiglas.

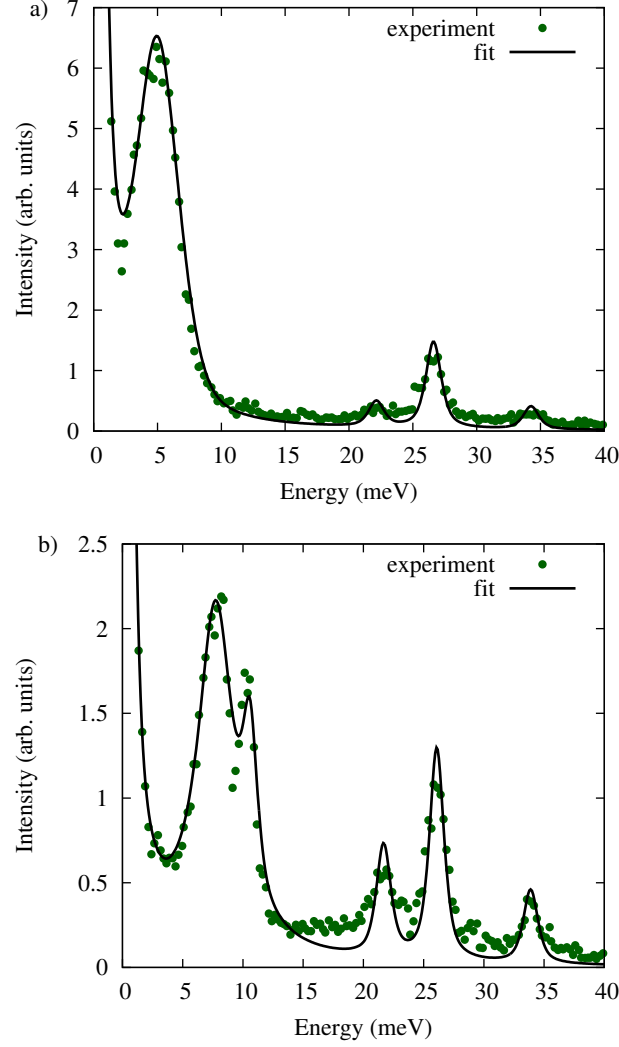$$f_{pV} = (1 - \eta) f_G(x;\Gamma) + \eta f_L(x;\Gamma) \tag{1}$$

FIG. 1. (color online) Energy scan at constant-Q at a) $Q = (0.0, 0, 8.3)$ and b) $Q = (0.0, 0, 8.5)$ measured at room temperature on LaFeAsO. Experimental data are given by solid green points. The black line is fit using a pseudo-Voigt function.

TABLE I. Theoretically relaxed and experimentally observed z-position for La and As atoms at room temperature, and the associated magnetic moment per Fe atom and total energy. In each case the room temperature experimental lattice parameters of ($a = 4.03533$Å, $c = 8.74090$Å) were used.[20,21]

	NM	SDW	Striped	Checkerboard	Exp.[20,21]
z_{La}	0.13993	0.13875	0.13883	0.13887	0.14154
z_{As}	0.63829	0.64820	0.64770	0.64401	0.6512
μ_{Fe}	0.0	2.32	2.30	1.91	0.36-0.78
E(Ry)	0.0	-0.032	-0.033	-0.009	

Figure 1 shows a line scan consisting of several phonon excitations at $\mathbf{Q} = (0, 0, 8.3)$ and $\mathbf{Q} = (0, 0, 8.5)$ at room temperature. The peak positions for these and other scans were obtained from fits and used to construct the dispersion of phonon branches along the different scan directions, as shown in Fig. 2. The intensity of the phonon modes multiplied by the frequency is also represented in Fig. 2 by the diameter of the circles.

In order to understand the features of the phonon dispersion, the experimental measurements were compared to *ab initio* calculations of the phonons. The phonon dispersion was calculated using DFT and Density Functional Perturbation Theory (DFPT).[22] There are significant differences in the experimental lattice parameters and parameters

from the "relaxed" structure with the lowest calculated energy. Also, in spin-polarized calculations with the experimentally observed AFM order, the lattice distorts into the orthorhombic Cmma structure observed experimentally at lower temperatures. With these difficulties in mind, the experimental lattice parameters at room temperature in the tetragonal phase ($a = 4.03533$Å , $c = 8.74090$Å) were used for all calculations.[20,21] In addition, there is debate over the appropriate internal z-parameter to use for the position of lanthanum and arsenic atoms.[2;9,23,24] For better accuracy of the calculated phonons, we chose the calculated relaxed positions where all forces were zero. Structural parameters used for the non-magnetic and spin-polarized calculations as well as experimental measurements are given in table I. The pseudopotentials chosen used the Perdew-Burke-Ernzerhof (PBE) exchange correlation functional.[25,26] Settings of an 8x8x4 (nonmagnetic), 4x4x4 (striped & SDW) and 8x8x2 (checkerboard) k-mesh and 50 Ry and 660 Ry energy cutoffs for the wavefunctions and charge density were chosen to ensure meV precision of the calculated phonon dispersion. These parameters are similar to other phonon calculations of LaFeAsO.[27,28] Phonon frequencies were calculated on either a 4x4x2 (nonmagnetic), 2x2x2 (striped & SDW) or 4x4x1 (striped) q-mesh and then interpolated along several symmetry directions. The resulting phonon frequencies and eigenvectors were used to calculate the dynamical structure factor along the selected scan directions. The dynamical structure factor, which is proportional to the x-ray scattering intensity, is given in Eqn. 2.[29–31] In these equations, $W_d(\mathbf{Q})$ is the Debye-Waller factor, $n_j(\mathbf{q})$ is the Bose-Einstein distribution, $f_d(\mathbf{Q})$ is the x-ray form factor, and $\sigma_{\mathbf{d}}^j(\mathbf{q})$ is the eigenvector corresponding to the normalized motion of atom d in the jth phonon branch. While the DFT calculation does not include temperature dependence, the Bose-Einstein distribution was set to 300K.

$$S_j(\mathbf{q}, \omega) = \frac{\left|H_{\mathbf{q}}^j(\mathbf{Q})\right|^2}{2\omega_j(\mathbf{q})}(1 + n_j(\mathbf{q}))\,\delta\{\omega - \omega_j(\mathbf{q})\} \tag{2a}$$

$$H_{\mathbf{q}}^j(\mathbf{Q}) = \sum_d \frac{f_d(\mathbf{Q})}{\sqrt{M_d}}\exp\left(-W_d(\mathbf{Q}) + i\mathbf{Q}\cdot\mathbf{d}\right)\left\{\mathbf{Q}\cdot\sigma_d^j(\mathbf{q})\right\} \tag{2b}$$

$$W_d(\mathbf{Q}) = \frac{\hbar}{4M_d\Omega_{BZ}}\int_{\Omega_{BZ}}\sum_j \frac{|\mathbf{Q}\cdot\sigma_d^j(\mathbf{q})|}{\omega_j}\langle 2n_j(\mathbf{q}) + 1\rangle \tag{2c}$$

Both the x-ray form factor and the Debye-Waller factor decrease intensity of the phonon excitations with increasing Q. The preferred approach for computer applications are numerical approximations to the x-ray form factor. The x-ray form factor has been parameterized by Waazmaier and Kirfel as the sum of five Gaussians plus a constant term.[32] The Debye-Waller factor, calculated using Eqn. 2c, can be thought of as the mean-squared value of the displacement each atom dotted with $\mathbf{Q}$. The volume integral was calculated using the tetrahedron method[33,34] on a 16x16x8 (nonmagnetic), 16x16x4 (checkerboard) and 12x12x12 (SDW & striped) Monkhorst-Pack q-point grid.[35] To second order, the integral over the tetrahedron is simply the function evaluated at the center point multiplied by the volume. To avoid repeating the calculation for each value of Q, the nine potential components of the phonon eigenvector were stored and the dot product calculated later.

The delta function in ω was convoluted with the elastic scattering width of Plexiglas measured on the same analyzer. The pseudo-Voigt function fits well to the center of each peak, but small discrepancies exist in the tail. To minimize this effect a discrete linear convolution between the raw experimental data and simulated delta functions (single point on a grid) was performed numerically.

In addition to the energy resolution, the diameter of the analyzer leads to a finite resolution in $\mathbf{Q}$. Slightly different positions on the analyzer can be described by a radial component, determined from the size of the analyzer (10 cm) and the distance from the sample to the analyzer (9 m), and an angular component covering the entire circle. Values of $\mathbf{Q}$ accepted by the analyzer can be written as a function of these two variables. 5000 samples from a pseudo-random number generator gave sufficient precision for convolution of constant-$\mathbf{Q}$ scans with the $\mathbf{Q}$-space resolution. Due to the lower required precision 1000 samples were used for each contour plot.

Figure 1 shows a constant-$\mathbf{Q}$ energy scan at $(0, 0, 8.3)$ and $(0, 0, 8.5)$ at room temperature. Experimental data are given by the green points and pseudo-Voigt fits by the solid black line. The default values for η and Γ only account for the energy resolution. In general, we found the acoustic modes are much broader than the resolution width and fits of the acoustic modes are adjusted by including η and Γ as variables. At (0,0,8.3), optical modes are present at 22, 27, and 34 meV. At (0,0,8.5) the acoustic mode and a nearby optical mode is present at 8 and 11 meV, along with three other modes at 22, 26 and 34 meV, respectively. Over the entire range measured, η varying between 0.48 and 1.0 and Γ varrying between 1.85 and 3.96. The fitted values for each scan of the acoustic branch given in table II

Fig. 3 shows several calculations of the dynamical structure factor at $\mathbf{Q}=(0, 0, 8.5)$ which can be directly compared to Fig. 1b. The red dotted line is a non-magnetic calculation. Frequencies for the acoustic and lowest optical modes are reasonable, but the calculated intensity of the optical mode is too high. Attempts to include the experimental uncertainty in $\mathbf{Q}$ could not reproduce the observed broadening of the acoustic mode, meaning it is not an artifact of
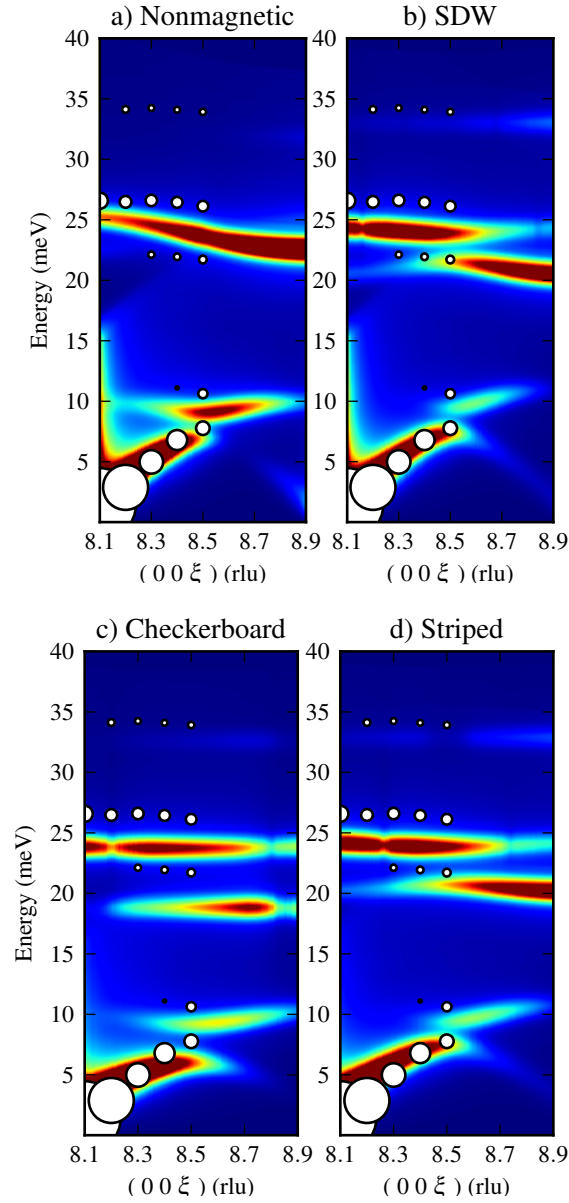
FIG. 2. (color online) Contour plots of the calculated dynamical structure factor along (0,0,L). Values range from blue (no intensity) to red (high intensity), and have been multiplied by the energy to improve visibility of the optical modes. The white dots show the experimentally determined frequencies, as described in the text, with the intensity (also multiplied by the frequency) shown by the size of the dot. a) Nonmagnetic calculation b) SP calculation with SDW ordering, c) SP calculation with checkerboard ordering. d) SP calculation with striped ordering.

TABLE II. Measured frequency and peak shape of the longitudinal acoustic mode along 00L

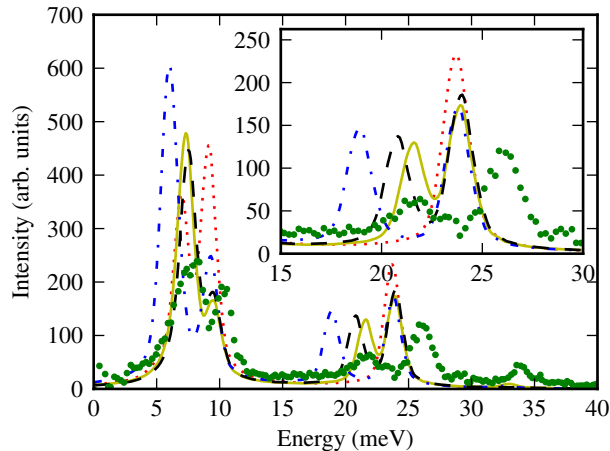| L	ω (meV)	Γ (meV)	η
8.1	1.5	1.85±0.03	0.76±0.02
8.2	2.9	3.27±0.05	0.66±0.04
8.3	5.0	3.96±0.09	0.47±0.07
8.4	6.8	3.50±0.08	0.73±0.06
8.5	7.8	3.67±0.12	1.0

FIG. 3. (color online) Dynamical structure factor calculation of constant-Q line scan at $Q = (0, 0, 8.5)$. The dotted red line corresponds to non-magnetic calculations of the dynamical structure factor. The solid yellow line corresponds to spin-polarized calculations imposing the SDW AFM ordering observed at lower temperatures. The black dashed line and blue dashed-dotted lines correspond to spin-polarized calculations with a striped (ferromagnetic along c) and checkerboard ordering, respectively. The elastic peak as been subtracted from the experimental data, shown in green circles, and is normalized to the average of the four calculations. The inset zooms in on the anomalous modes near 24 meV.

Q-space resolution. The phonon excitation near 24 meV consists of two modes separated by 0.2 meV. At the zone boundary, lower and upper A_{1g} modes consist of As and La motion, respectively, polarized along the c-axis. At the zone center, these modes are mixed, each containing both La and As motion and the upper mode contributes 80% of the structure factor. This result from the nonmagnetic calculation is inconsistent with the measurements, where these two modes are clearly split by 4 meV at (0,0,8.5). Other calculated frequencies agree with recently published phonon dispersions,[27,28] although they are generally a few meV lower in energy than observations. Small changes in lattice parameters are not responsible, as an unphysical 7% reduction in the unit cell volume is required to stiffen this phonon mode in the nonmagnetic calculation to the observed value. While this discrepancy exposes limits on the accuracy of these DFT calculations, this should not detract from qualitative changes between calculations, such as the splitting of the A_{1g} branches, that are also observed experimentally. At both values of Q, the 32 meV feature consists of both Fe and As motion, but the intensity is extremely weak.

In the spin-polarized calculation corresponding to the observed stripe AFM structure (Fig. 4b), the effect of the Fe magnetization is to strongly split the two 24 meV branches at (0,0,8.5) with the 21 meV excitation, containing As motion, lowering in energy by approximately 8.6%. The ratio of intensities between the acoustic and nearby optical mode moves in the direction of, though slightly more than, what is observed experimentally. The 24 meV peak is primarily La motion. The intensity of the 32meV feature is 5.2 times stronger, in better agreement with experiment.

In order to better understand the importance of the specific magnetic order and size of the Fe moment on the lattice dynamics, two additional calculations were performed in hypothetical magnetic structures. First is the "checkerboard" magnetic structure, shown in Fig. 4c. It is a tetragonal space group, where Fe neighbors have opposite spins. This calculation converges to a solution 0.023 Ry higher in energy with an 18% smaller magnetic moment per Fe atom. The acoustic mode is slightly softer and has greater intensity. The 21 meV excitation, containing As motion, is lower in energy by approximately 19.9%. The intensity of the 32meV feature is 2.9 times stronger than in the nonmagnetic calculation.

Second is the CeFeAsO structure,[36] also referred to as "striped," and shown in Fig. 4d. It is an orthorhombic space group with ferromagnetic coupling of Fe moments along the c-axis. The dynamical structure factor for this material is shown with black dashes in Fig. 3. The frequency and intensity of the acoustic and optical modes at 8 and 11 meV are nearly identical. Once again, the effect of the magnetization on Fe is to strongly split these branches, with the 21 meV excitation lowering in energy by approximately 11.9%. The intensity of the 32meV feature is half as strong as the nonmagnetic calculation.

Fig. 2 compiles all of the experimental data and calculations of the different magnetic structures by showing several contour plots of the dynamical structure factor along $(0, 0, L)$. Values of calculated intensities range from blue (low intensity) to red (high intensity), and have been multiplied by the energy to improve visibility of the optical modes. The white dots show the experimentally determined frequencies with the intensity shown by the size of the dot. In each
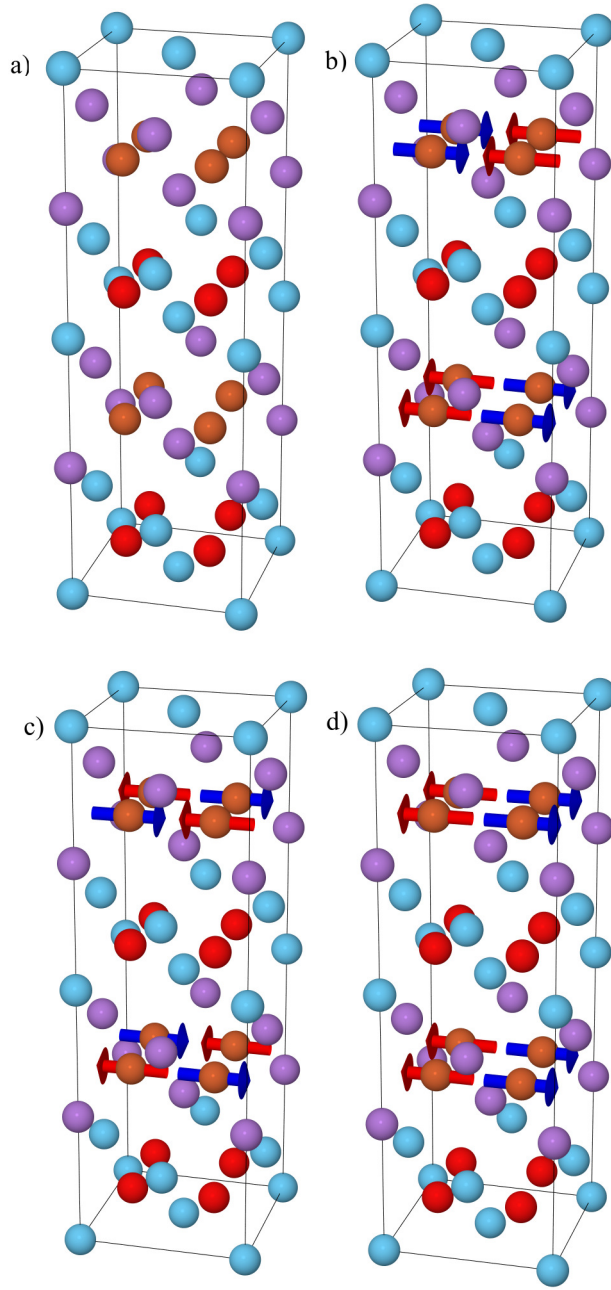
FIG. 4. (color online) Different AFM order used in the calculations. La atoms are light blue, O atoms green, As atoms purple and Fe atoms brown. The red and blue arrows show up and down spin, respectively. a) expanded non-magnetic unit cell, b) experimentally observed SDW, c) Checkerboard ordering d) striped ordering aligned ferromagnetically along the c-axis

case, calculations with a magnetic moment on the Fe show splitting between the two A_{1g} modes near 24 meV. At the zone center, the upper mode softens by 3.7 (SDW) - 5.3 (checkerboard) % and the lower mode softens by 9.1 (SDW) - 16.6 (checkerboard) %. Calculated frequencies of these two modes are a few meV lower than observed. Comparing nonmagnetic and spin-polarized calculations, the frequency of the upper La-As mode is essentially unchanged ($< 0.6\%$) at the zone boundary. The intensity of the lower mode is strongest near (0,0,9), and the intensity of the upper mode is strongest near (0,0,8). The frequency of the lower mode differs by 2 meV. The SDW calculation best matches the experimental frequency, but the checkerboard pattern best matches the observed splitting between these two modes. We note that the checkerboard ordering also introduces a pronounced softening of the longitudinal acoustic mode when compared to the non-magnetic calculation and other magnetically ordered structures. Finally, we point out that

the intensity of the optical mode near 10 meV is highest in nonmagnetic calculation. Overall changes in the phonon frequencies and intensities indicate the complex and subtle effects that magnetic ordering has on the lattice dynamics.

Despite the changes introduced by magnetic order, all the spectra are qualitatively similar for different magnetic alignments, and in better agreement with experiment compared with nonmagnetic calculations. This might be understood to occur as a consequence of Fe moments still being present above T_N, though without long-range order.[37–39] Compared to nonmagnetic calculations, imposing an AFM ordering better describes phonons in LaFeAsO. Consequently, it is likely that the presence of Fe moments, ordered or not, affects the force constants. Considering only c-axis polarized phonon branches containing La and As motion significantly reduces the number of force constants that contribute. First, only the "zz" term in the 3x3 force constant tensor can contribute, greatly simplifying comparisons between different magnetic unit cells. Fe and O are essentially stationary in the modes considered, meaning force constants between Fe-Fe,Fe-O and O-O atoms do not contribute. La-La and La-O force constants are essentially unchanged in each calculation, and the bond distance between La-Fe is large and the resulting force constant small. Therefore, we can limit ourselves to the "zz" term for La-As, As-As, and Fe-As force constants. Of these, the Fe-As force constant is the largest by an order of magnitude. Even with these simplifications, there was no clear softening of any specific pair-wise force. This provides additional evidence for T. Yildirim's observation that changes in the phonon modes are due to a complicated renormalization rather than softening of a single pair-wise force.[2] In the non-magnetic calculation the on-site force constants, which are a sum of all pair-wise interactions, are (in eV/Å^2) (11.2,11.2,8.9) for Fe and (10.5,10.5,9.6) for As. They show significant softening around 10-20% with the introduction of magnetic order, in good agreement with T. Yildirim's work. Small differences on the order of 0.2 eV/Å^2 or less in the on-site force constants are likely from slightly different lattice parameters chosen in our calculations.

In summary, we have measured the phonon dispersion along (0,0,L) in the tetragonal phase of LaFeAsO at room temperature, well above the magnetic ordering temperature of 138K. Nonmagnetic calculations fail to reproduce the observed splitting between two A_{1g} phonon modes at 22 and 26 meV. Spin-polarized first-principles calculations imposing a number of hypothetical antiferromagnetic orders are qualitatively similar and in better agreement with the experimental results than non-spin-polarized calculations. The presence of Fe-spins are necessary to predict the observed spectrum above T_N, however the renormalization of the force constants is quite complex and cannot be reduced to a single pair-wise force constant.

ACKNOWLEDGMENTS

[1] L. Boeri, O. V. Dolgov, and A. A. Golubov, Phys. Rev. Lett. **101**, 026403 (2008).

[2] T. Yildirim, Physica C: Superconductivity **469**, 425 (2009).

[3] A. D. Christianson, M. D. Lumsden, O. Delaire, M. B. Stone, D. L. Abernathy, M. A. McGuire, A. S. Sefat, R. Jin, B. C. Sales, D. Mandrus, E. D. Mun, P. C. Canfield, J. Y. Y. Lin, M. Lucas, M. Kresch, J. B. Keith, B. Fultz, E. A. Goremychkin, and R. J. McQueeney, Phys. Rev. Lett. **101**, 157004 (2008).

[4] S. Higashitaniguchi, M. Seto, S. Kitao, Y. Kobayashi, M. Saito, R. Masuda, T. Mitsui, Y. Yoda, Y. Kamihara, M. Hirano, and H. Hosono, Phys. Rev. B **78**, 174507 (2008).

[5] T. Fukuda, A. Q. R. Baron, S. ichi Shamoto, M. Ishikado, H. Nakamura, M. Machida, H. Uchiyama, S. Tsutsui, A. Iyo, H. Kito, J. Mizuki, M. Arai, H. Eisaki, and H. Hosono, Journal of the Physical Society of Japan **77**, 103715 (2008).

[6] I. I. Mazin and M. D. Johannes, Nature Physics **5**, 141 (2009).

[7] A. Kreyssig, M. A. Green, Y. Lee, G. D. Samolyuk, P. Zajdel, J. W. Lynn, S. L. Bud'ko, M. S. Torikachvili, N. Ni, S. Nandi, J. B. Leão, S. J. Poulton, D. N. Argyriou, B. N. Harmon, R. J. McQueeney, P. C. Canfield, and A. I. Goldman, Phys. Rev. B **78**, 184517 (2008).

[8] D. K. Pratt, Y. Zhao, S. A. J. Kimber, A. Hiess, D. N. Argyriou, C. Broholm, A. Kreyssig, S. Nandi, S. L. Bud'ko, N. Ni, P. C. Canfield, R. J. McQueeney, and A. I. Goldman, Phys. Rev. B **79**, 060510 (2009).

[9] S. E. Hahn, Y. Lee, N. Ni, P. C. Canfield, A. I. Goldman, R. J. McQueeney, B. N. Harmon, A. Alatas, B. M. Leu, E. E. Alp, D. Y. Chung, I. S. Todorov, and M. G. Kanatzidis, Phys. Rev. B **79**, 220511 (2009).

[10] D. Reznik, K. Lokshin, D. C. Mitchell, D. Parshall, W. Dmowski, D. Lamago, R. Heid, K.-P. Bohnen, A. S. Sefat, M. A. McGuire, B. C. Sales, D. G. Mandrus, A. Subedi, D. J. Singh, A. Alatas, M. H. Upton, A. H. Said, A. Cunsolo, Y. Shvyd'ko, and T. Egami, Phys. Rev. B **80**, 214534 (2009).

[11] R. Mittal, L. Pintschovius, D. Lamago, R. Heid, K.-P. Bohnen, D. Reznik, S. L. Chaplot, Y. Su, N. Kumar, S. K. Dhar, A. Thamizhavel, and T. Brueckel, Journal of Physics: Conference Series **251**, 012008 (2010).

[12] V. G. Hadjiev, M. N. Iliev, K. Sasmal, Y.-Y. Sun, and C. W. Chu, Phys. Rev. B **77**, 220505 (2008).

[13] C. Marini, C. Mirri, G. Profeta, S. Lupi, D. D. Castro, R. Sopracase, P. Postorino, P. Calvani, A. Perucchi, S. Massidda, G. M. Tropeano, M. Putti, A. Martinelli, A. Palenzona, and P. Dore, EPL (Europhysics Letters) **84**, 67013 (2008).

[14] J.-Q. Yan, S. Nandi, J. L. Zarestky, W. Tian, A. Kreyssig, B. Jensen, A. Kracher, K. W. Dennis, R. J. McQueeney, A. I. Goldman, R. W. McCallum, and T. A. Lograsso, Applied Physics Letters **95**, 222504 (2009).

[15] M. Le Tacon, T. R. Forrest, C. Rüegg, A. Bosak, A. C. Walters, R. Mittal, H. M. Rønnow, N. D. Zhigadlo, S. Katrych, J. Karpinski, J. P. Hill, M. Krisch, and D. F. McMorrow, Phys. Rev. B **80**, 220504 (2009).

[16] A. H. Said, H. Sinn, and R. Divan, Journal of Synchrotron Radiation **18**, 492 (2011).

[17] T. S. Toellner, A. Alatas, and A. H. Said, Journal of Synchrotron Radiation **18**, 605 (2011).

[18] C. de la Cruz, Q. Huang, J. W. Lynn, J. Li, W. R. II, J. L. Zarestky, H. A. Mook, G. F. Chen, J. L. Luo, N. L. Wang, and P. Dai, Nature **453**, 899 (2008).

[19] H.-H. Klauss, H. Luetkens, R. Klingeler, C. Hess, F. J. Litterst, M. Kraken, M. M. Korshunov, I. Eremin, S.-L. Drechsler, R. Khasanov, A. Amato, J. Hamann-Borrero, N. Leps, A. Kondrat, G. Behr, J. Werner, and B. Büchner, Phys. Rev. Lett. **101**, 077005 (2008).

[20] Y. Kamihara, T. Watanabe, M. Hirano, and H. Hosono, Journal of the American Chemical Society **130**, 3296 (2008).

[21] D. C. Johnston, Advances in Physics **59**, 803 (2010).

[22] P. Giannozzi, S. Baroni, N. Bonini, M. Calandra, R. Car, C. Cavazzoni, D. Ceresoli, G. L. Chiarotti, M. Cococcioni, I. Dabo, A. Dal Corso, S. de Gironcoli, S. Fabris, G. Fratesi, R. Gebauer, U. Gerstmann, C. Gougoussis, A. Kokalj, M. Lazzeri, L. Martin-Samos, N. Marzari, F. Mauri, R. Mazzarello, S. Paolini, A. Pasquarello, L. Paulatto, C. Sbraccia, S. Scandolo, G. Sclauzero, A. P. Seitsonen, A. Smogunov, P. Umari, and R. M. Wentzcovitch, Journal of Physics: Condensed Matter **21**, 395502 (2009).

[23] R. Mittal, L. Pintschovius, D. Lamago, R. Heid, K.-P. Bohnen, D. Reznik, S. L. Chaplot, Y. Su, N. Kumar, S. K. Dhar, A. Thamizhavel, and T. Brueckel, Phys. Rev. Lett. **102**, 217001 (2009).

[24] R. Mittal, R. Heid, A. Bosak, T. R. Forrest, S. L. Chaplot, D. Lamago, D. Reznik, K.-P. Bohnen, Y. Su, N. Kumar, S. K. Dhar, A. Thamizhavel, C. Rüegg, M. Krisch, D. F. McMorrow, T. Brueckel, and L. Pintschovius, Phys. Rev. B **81**, 144502 (2010).

[25] We used the pseudopotentials La.pbe-nsp-van.UPF, Fe.pbe-paw_kj.UPF, As.pbe-n-van.UPF and O.pbe-van_ak.UPF from the http://www.quantum-espresso.org distribution.

[26] J. P. Perdew, K. Burke, and M. Ernzerhof, Phys. Rev. Lett. **77**, 3865 (1996).

[27] D. J. Singh and M.-H. Du, Phys. Rev. Lett. **100**, 237003 (2008).

[28] L. Boeri, O. V. Dolgov, and A. A. Golubov, Phys. Rev. Lett. **101**, 026403 (2008).

[29] S. W. Lovesey, *Theory of Neutron Scattering From Condensed Matter*, International Series of Monographs on Physics, Vol. 1 (Oxford University Press, 1984).

[30] A. Q. R. Baron, Journal of The Spectroscopical Society of Japan **58**, 205 (2009), (in Japanese) / arXiv:0910.5764 (in English).

[31] E. Burkel, Reports on Progress in Physics **63**, 171 (2000).

[32] D. Waasmaier and A. Kirfel, Acta Crystallographica Section A **51**, 416 (1995).

[33] D. Zaharioudakis, Computer Physics Communications **157**, 17 (2004).

[34] P. E. Blöchl, O. Jepsen, and O. K. Andersen, Phys. Rev. B **49**, 16223 (1994).

[35] H. J. Monkhorst and J. D. Pack, Phys. Rev. B **13**, 5188 (1976).

[36] J. Zhao, Q. Huang, C. de La Cruz, S. Li, J. W. Lynn, Y. Chen, M. A. Green, G. F. Chen, G. Li, Z. Li, J. L. Luo, N. L. Wang, and P. Dai, Nature Materials **7**, 953 (2008).

[37] S. O. Diallo, D. K. Pratt, R. M. Fernandes, W. Tian, J. L. Zarestky, M. Lumsden, T. G. Perring, C. L. Broholm, N. Ni, S. L. Bud'ko, P. C. Canfield, H.-F. Li, D. Vaknin, A. Kreyssig, A. I. Goldman, and R. J. McQueeney, Phys. Rev. B **81**, 214407 (2010).

[38] S. Wakimoto, K. Kodama, M. Ishikado, M. Matsuda, R. Kajimoto, M. Arai, K. Kakurai, F. Esaka, A. Iyo, H. Kito, H. Eisaki, and S. ichi Shamoto, Journal of the Physical Society of Japan **79**, 074715 (2010).

[39] M. Ishikado, R. Kajimoto, S.-i. Shamoto, M. Arai, A. Iyo, K. Miyazawa, P. M. Shirage, H. Kito, H. Eisaki, S. Kim, H. Hosono, T. Guidi, R. Bewley, and S. M. Bennington, ArXiv e-prints (2008), arXiv:0809.5128 [cond-mat.supr-con].